Gut flora disequilibrium promotes the initiation of liver cancer by modulating tryptophan metabolism and up-regulating SREBP2

Wen Chen[a,b,c,1], Liang Wen[a,b,c,d,1] (ID), Yingying Bao[a,b,c], Zengwei Tang[a,b,c] (ID), Jianhui Zhao[a,b,c] (ID), Xiaozhen Zhang[a,b,c], Tao Wei[a,b,c,d], Jian Zhang[a,b,c,d], Tao Ma[a,b,c,d], Qi Zhang[a,b,c,d], Xiao Zhi[a,b,c,d], Jin Li[a,b,c], Cheng Zhang[a,b,c] (ID), Lei Ni[a,c], Muchun Li[a,c], and Tingbo Liang[a,b,c,d,2] (ID)

The gut microbiota and liver cancer have a complex interaction. However, the role of gut microbiome in liver tumor initiation remains unknown. Herein, liver cancer was induced using hydrodynamic transfection of oncogenes to explore liver tumorigenesis in mice. Gut microbiota depletion promoted liver tumorigenesis but not progression. Elevated sterol regulatory element-binding protein 2 (SREBP2) was observed in mice with gut flora disequilibrium. Pharmacological inhibition of SREBP2 or *Srebf2* RNA interference attenuated mouse liver cancer initiation under gut flora disequilibrium. Furthermore, gut microbiota depletion impaired gut tryptophan metabolism to activate aryl hydrocarbon receptor (AhR). AhR agonist Ficz inhibited SREBP2 posttranslationally and reversed the tumorigenesis in mice. And, AhR knockout mice recapitulated the accelerated liver tumorigenesis. Supplementation with *Lactobacillus reuteri*, which produces tryptophan metabolites, inhibited SREBP2 expression and tumorigenesis in mice with gut flora disequilibrium. Thus, gut flora disequilibrium promotes liver cancer initiation by modulating tryptophan metabolism and up-regulating SREBP2.

gut microbiota | liver tumorigenesis | SREBP2 | tryptophan metabolism | AhR

Primary liver cancer is currently the sixth most common cancer and fourth leading cause of cancer-related death globally (1). The well-established risk factors include chronic hepatitis C virus or hepatitis B virus infection, nonalcoholic fatty liver disease (NAFLD), alcohol consumption, and diabetes. As one of the hallmarks of cancer (2), the gut microbiota has been widely recognized to play a key role in liver cancer (3). Most studies focused on the relationship between the gut microbiota and liver cancer development. Lipopolysaccharide (LPS) is one of the most studied bacterial components, and its receptor, toll-like receptor 4 (TLR4), was reported to be required for liver tumor promotion, but not for liver tumor initiation (4). It has been reported that secondary bile acid, a microbiome-derived metabolite, is critical in mediating host immunity in tumor progression. And, gut sterilization effectively attenuates liver tumor progression (5). In nonalcoholic steatohepatitis-associated hepatocellular carcinoma (HCC), the gut microbiota promotes HCC progression via suppression of antitumor immunity (6). However, there is little evidence for the role of gut commensal bacteria in liver tumor initiation.

The crosstalk between liver and gut regulates metabolism and immune functions mutually. Increasing evidence indicates that gut commensal bacteria play an important role in liver tumor progression by regulating host antitumor immunity (7). More importantly, the gut microbiota influences liver metabolism via its metabolites. Among them, cholesterol metabolism is regulated by the gut microbiota (8, 9), and its homeostasis is inextricably bound with liver cancer (3). The mevalonate pathway has been reported to be integral to tumor initiation and progression (10). In liver cancer, p53 blocks the activation of sterol regulatory element-binding protein 2 (SREBP2), the master transcriptional regulator of the mevalonate pathway, to suppress tumorigenesis (11). Moreover, dietary cholesterol drives NAFLD–HCC formation by inducing alteration of the gut microbiota and metabolites in mice (12). However, it remains unclear whether aberrant cholesterol metabolism induced by gut flora disequilibrium affects liver tumorigenesis and the underlying mechanism.

In the present study, using the hydrodynamic transfection-induced liver cancer model (13), we found that gut flora disequilibrium induced by antibiotics dramatically promoted the initiation of liver cancer and liver cholesterol synthesis. Gut flora disequilibrium-induced liver cholesterol metabolism was relevant to tryptophan metabolites in the gut, as well as the activation of their receptor, aryl hydrocarbon receptor (AhR), in the liver. Therefore, the present study was performed to determine the role and the associated molecular mechanisms of gut flora disequilibrium in the initiation of liver cancer.

Significance

Primary liver cancer is currently the sixth most common cancer and fourth leading cause of cancer-related death globally. The limited therapeutic options and poor prognosis of patients with primary liver cancer highlight the significance of developing cancer prevention strategies. Our findings identified a mechanism of gut flora disequilibrium-promoted liver cancer initiation via a tryptophan metabolism-balanced AhR-SREBP2 axis between the gut and liver. Our results might contribute to developing strategies for liver cancer prevention through gut flora manipulation.

Results

Gut Flora Disequilibrium Promoted Liver Tumor Initiation in Mice. To determine the role of gut commensal bacteria in liver tumor initiation, mice were administered with an antibiotic cocktail (ABX) (vancomycin, neomycin, and ampicillin) in drinking water to deplete the gut commensal bacteria. We first examined changes in fecal bacterial community by 16S rRNA sequencing after 14 d of ABX treatment (*SI Appendix*, Fig. S1*A*). At the phylum level, the relative abundances of *Bacteroidetes* and *Firmicutes* significantly decreased, with *Proteobacteria* accounting for the vast majority of total bacteria following ABX treatment (*SI Appendix*, Fig. S1*B*). The *Lactobacillus* genus represented the second largest proportion of the bacteria (23.5%) in normal mice, which was significantly reduced in ABX-treated mice. And, *Lactobacillus intestinalis* represented the significantly reduced species of *Lactobacillus* between the control and ABX groups (*SI Appendix*, Fig. S1 *C* and *D*). The hydrodynamic tail vein injection (HTVi)-induced HCC model was constructed by cotransfection of two oncogenes, human c-Myc and n-RAS (Ras/Myc), which was performed at 2 wk after ABX treatment, and mice were killed for phenotypic analysis at 6 wk (Fig. 1*A*). The tumor burden was assessed by analysis of liver weight/body weight (LW/BW) ratios, tumor number, and spleen weight/body weight (SW/BW) ratios, as well as histological staining of hematoxylin–eosin H&E and Ki67. ABX treatment significantly accelerated Ras/Myc-induced liver tumor initiation when the tumor nodules developed for 4 wk (Fig. 1 *B* and *C*), or as short as 2 and 3 wk (*SI Appendix*, Fig. S2 *A–D*, respectively). Mouse survival analysis showed that ABX-treated mice had a significantly shorter mean survival time compared with that of the control mice after tumor initiation by Ras/Myc transfection (Fig. 1*D*). We also tested whether short-term gut microbiome depletion caused a difference in tumor initiation. The result revealed a similar effect if ABX treatment was stopped early (1 wk after HTVi) (*SI Appendix*, Fig. S2 *E–G*). To further confirm this phenotype, other liver tumor models were also applied. The mice were transfected with human c-Met and human β-Catenin oncogenes after 2 wk of gut microbiome depletion and killed at 6 wk (Fig. 1*E*). The same effect of ABX treatment was observed upon macroscopic and histological examination. Increased LW/BW ratios, tumor number, and SW/BW ratios were also observed in the ABX-treated mice (Fig. 1 *F* and *G*). To exclude the effect of ABX treatment-induced low LW/BW ratio (92.97% of that in the control mice) in tumor initiation (*SI Appendix*, Fig. S2*H*), ABX-treated mice were given 90% of the volume of that given to the control mice by HTVi, and significantly increased tumor burdens were still observed in mice with gut microbiome depletion (*SI Appendix*, Fig. S2 *I* and *J*). We further established the intrahepatic cholangiocarcinoma (ICC) model by cotransfection of two oncogenes, human Yes-Associated Protein (YAP) and the serine/threonine kinase AKT (YAP/AKT), to investigate whether gut microbiome also affected the initiation of ICC (*SI Appendix*, Fig. S3*A*). Consistent with mouse models of HCC, ABX treatment also significantly accelerated the initiation of ICC compared to that in control mice (*SI Appendix*, Fig. S3 *B* and *C*).

To further assess the role of the gut microbiome in liver tumor initiation, germ-free (GF) mice were used to make the gut microbiota fully depleted. HTVi (Ras/Myc) was performed in GF and normal specified-pathogen-free (SPF) mice, which were killed at 8 wk (*SI Appendix*, Fig. S4*A*). Consistent with ABX treatment, the GF mice exhibited significantly faster tumor formation with increased LW/BW ratios, tumor number, and SW/BW ratios, compared with those in the SPF mice (*SI Appendix*, Fig. S4 *B* and *C*). Furthermore, we performed fecal microbiome transplantation (FMT) to investigate whether the fecal microbiome from normal SPF mice could slow down liver tumor initiation in GF mice (Fig.1*H*). 16S rRNA sequencing and restored cecum size confirmed that fecal microbiome from SPF mice was successfully colonized in GF + FMT mice (*SI Appendix*, Fig. S4 *D–G*). The increased tumor formation in the GF mice was inhibited by FMT, including a reduced LW/BW ratio, reduced tumor number, and a decreased SW/BW ratio (Fig. 1 *I* and *J*). Taken together, these findings suggested that the gut commensal microbiota inhibited liver tumor initiation in mice.

Gut Flora Disequilibrium Failed to Affect Tumor Progression and Metastasis in Mice. Increasing evidence points toward a key role of the bacterial microbiome in promoting the development of HCC (3). Therefore, we used the HTVi-induced liver cancer model to explore the role of gut commensal bacteria in liver tumor progression. ABX treatment was given 2 wk after HTVi (Ras/Myc) when there were macroscopic minimal tumors on the liver surface, and the mice were killed 6 wk after HTVi (Fig. 2*A*). The result showed that after tumor initiation, instead of tumor promotion, gut commensal bacteria depletion in mice induced a slight decrease in tumor number ($P = 0.043$) and a decreasing trend of the LW/BW ratio ($P = 0.081$) and SW/BW ratio ($P = 0.100$) (Fig. 2 *B* and *C*). We also explored the effect of gut flora disequilibrium in liver cancer metastasis and other type of metastatic cancer in the liver. We used the subcutaneously implanted tumor model (Hep1-6, a mouse HCC cell line) (Fig. 2*D*) and found no differences in tumor weight and tumor volume between ABX-treated mice and control mice (Fig. 2 *E* and *F*). To establish the liver metastasis model, intrasplenic injection of Kras$^{LSL-G12D}$, Trp53$^{LSL-R172H}$, Pdx1-Cre (KPC) pancreatic tumor cells was performed (Fig. 2*G*), and there was no difference in liver metastasis between ABX-treated mice and control mice (Fig. 2 *H* and *I*). The same result was also found in liver cancer lung metastasis induced by peripheral injection of Hep1-6 cells (Fig. 2 *J–L*). In summary, in contrast to liver cancer initiation, gut flora disequilibrium failed to affect tumor progression and metastasis in mice.

Gut Flora Disequilibrium Led to Increased SREBP2 and Downstream Cholesterol Synthesis-Related Gene Expression in the Liver. The divergent roles of gut commensal bacteria in liver cancer initiation and progression prompted us to explore the key driving genes in tumor initiation in the liver. Liver tissues from ABX-treated mice and control mice were isolated (Fig. 3*A*) and transcriptome analysis was performed. We identified 114 up-regulated genes and 114 down-regulated genes in livers of mice with ABX treatment compared to control mice (Fig. 3*B*). Gene Ontology-Biological Process analysis revealed enrichment of processes related to cholesterol metabolism (Fig. 3*C*). Pathway enrichment analysis in the Reactome database also revealed that "metabolism of steroids" and "cholesterol biosynthesis" pathways were up-regulated in mice with gut commensal bacteria depletion (Fig. 3*D*). Indeed, from the transcriptome analysis, the expression levels of many genes involved in cholesterol biosynthesis were up-regulated in the liver after ABX treatment (Fig. 3*E*). Then, real-time qRT-PCR and Western blotting were performed to validate some of the key cholesterol biosynthesis-related genes and proteins, respectively, which were mostly up-regulated in livers of ABX-treated mice (Fig. 3 *F* and *G*), which was also consistent with their expression in the liver of GF mice (*SI Appendix*, Fig. S5 *A* and *B*). Among them, the transcription factor SREBP2 (encoded by *Srebf2*) is known to be critical to control the expression of many downstream cholesterol biosynthesis-related genes. However, the mRNA expression of *Srebf2* did not change in the liver of mice with ABX treatment or in the GF mice (Fig. 3*F* and *SI Appendix*, Fig. S5*A*).
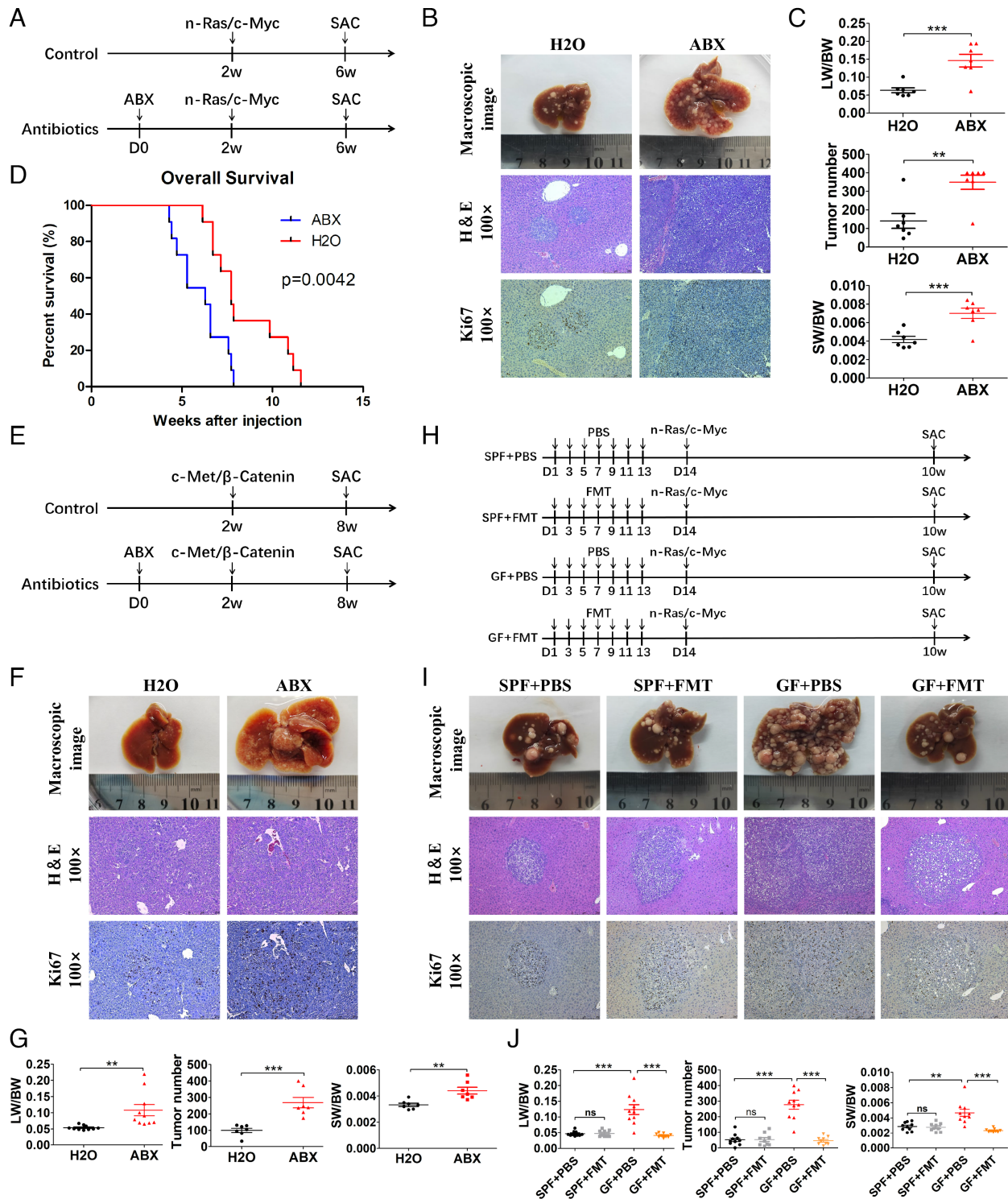
Fig. 1. Gut commensal bacteria depletion promoted liver tumor initiation in mice. (*A*) Experimental procedure (n = 7 per group). (*B*) Representative macroscopic views of livers, H&E staining, and immunohistochemistry (IHC) of Ki67 in mouse HCCs. (*C*) The LW/BW ratio, tumor number, and the SW/BW ratio of each group. (*D*) Survival curves of mice fed with antibiotics or H₂O in the N-Ras/c-Myc HCC model (n = 11 per group). (*E*) Experimental procedure of the C-Met/β-Catenin HCC model (n = 10 per group). (*F*) Representative macroscopic views of livers, H&E staining, and IHC of Ki67 in mouse HCCs (C-Met/β-Catenin model). (*G*) The LW/BW ratio, tumor number, and the SW/BW ratio of each group (C-Met/β-Catenin model). (*H*) Experimental procedure of FMT (SPF + PBS, n = 10; SPF + FMT, n = 9; GF + PBS, n = 10; GF + FMT, n = 9). (*I*) Representative macroscopic views of livers, H&E staining, and IHC of Ki67 in mouse HCCs. (*J*) The LW/BW ratio, tumor number, and the SW/BW ratio of each group. Data were presented as mean ± SEM, *P* values were calculated by Student's *t* test. ns, not significant; **P* <0.01; ***P* <0.001.

We then validated whether SREBP2 was up-regulated at the protein level in the liver in mice with ABX depletion and in the GF mice. The protein levels of both the precursor form of SREBP2 (p-SREBP2) and nuclear form of SREBP2 (n-SREBP2) were dramatically elevated in the livers of ABX-treated mice (Fig. 3*G*). The same results were observed in GF mice (*SI Appendix*, Fig. S5*B*). Moreover, cholesterol and triglycerides (TG) were measured in serum and liver samples. The concentrations of cholesterol were significantly elevated in the serum and liver of mice treated with ABX, and the concentrations of TG showed no significant
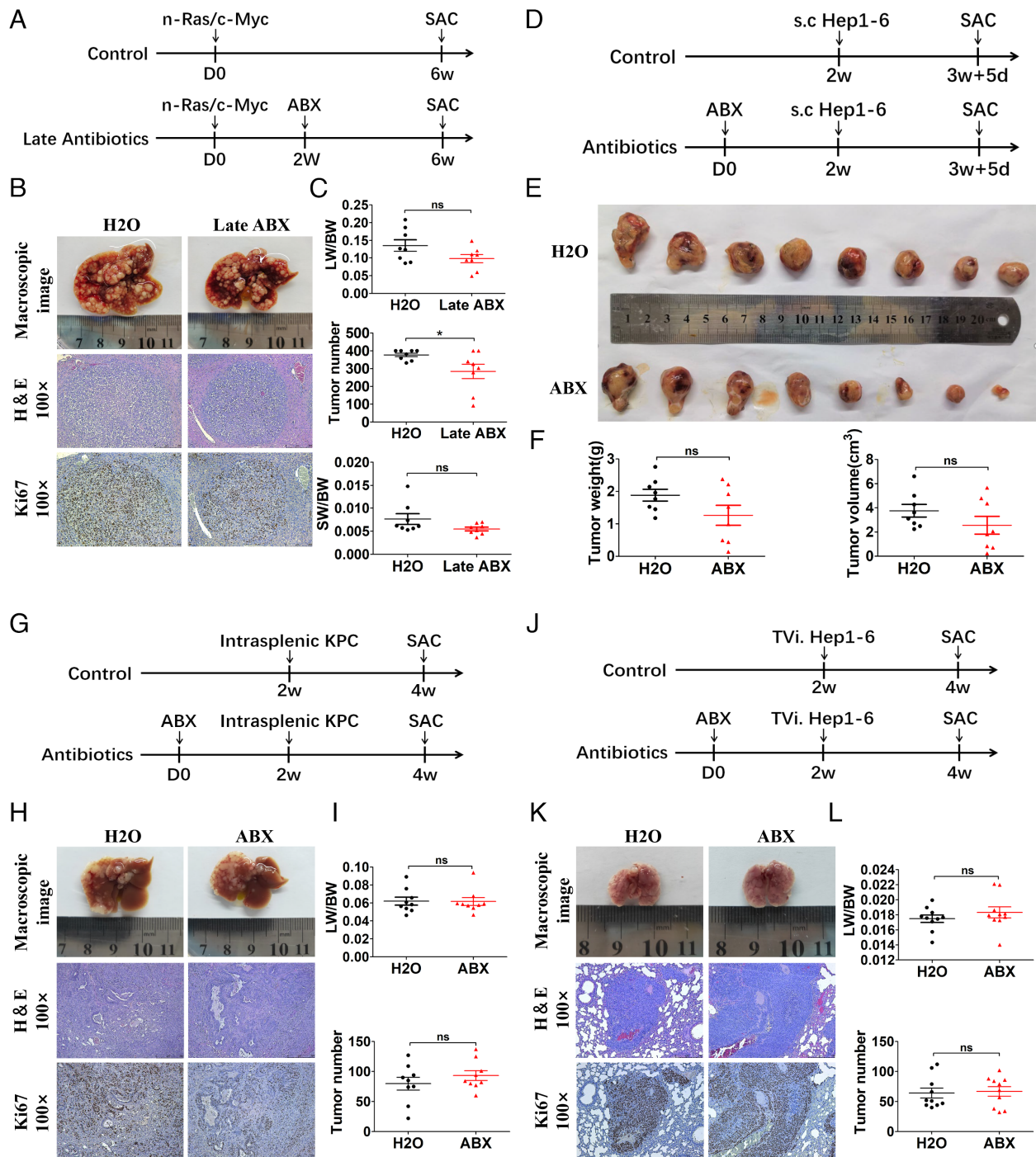
Fig. 2. Gut commensal bacteria depletion does not accelerate liver tumor progression in mice. (*A*) Experimental procedure (n = 8 per group). (*B*) Representative macroscopic views of livers, H&E staining, and IHC of Ki67 in mouse HCCs. (*C*) The LW/BW ratio, tumor number, and the SW/BW ratio of each group. (*D*) Experimental procedure (n = 8 per group). Mice were treated with antibiotics or H_2O for 2 wk before receiving subcutaneous injection of Hep1-6 tumor cell and, 12 d later, subcutaneous tumors were determined. (*E*) Macroscopic views of tumors. (*F*) Tumor weight and tumor volume of each group. (*G*) Experimental procedure (n = 9 per group). Mice were treated with antibiotics or H_2O for 2 wk before receiving intrasplenic injection of KPC tumor cells and, 2 wk later, liver metastases were determined. (*H*) Representative macroscopic views of livers, H&E staining, and IHC of Ki67 in mouse liver metastases. (*I*) The LW/BW ratio and tumor number of each group were determined. (*J*) Experimental procedure (n = 10 per group). Mice were treated with antibiotics or H_2O for 2 wk before receiving tail vein injection of Hep1-6 tumor cells and, 2 wk later, lung metastases were determined. (*K*) Representative macroscopic views of lungs, H&E staining, and IHC of Ki67 in mouse lung metastases. (*L*) The lung-body weight ratio (LW/BW) and tumor number of each group. Data were presented as mean ± SEM, *P* values were calculated by Student's *t* test. ns, not significant; *P <0.05.

differences between the two groups (Fig. 3*H*). Moreover, the liver function measurements revealed that ABX treatment had no toxic effect on the mouse liver (Fig. 3*I*). Taken together, gut flora disequilibrium led to increased SREBP2 and cholesterol synthesis-related gene expression in the liver, which supposed to be the key factor promoting liver cancer initiation.

Elevated Liver SREBP2 Promoted Liver Tumorigenesis in Mice with Gut Flora Disequilibrium. We then tried to address whether the enhanced cholesterol anabolism plays the pivotal role in liver tumor initiation. Studies on the influence of cholesterol metabolism in cancer progression highlighted the important effects of cholesterol metabolites on the tumor immune
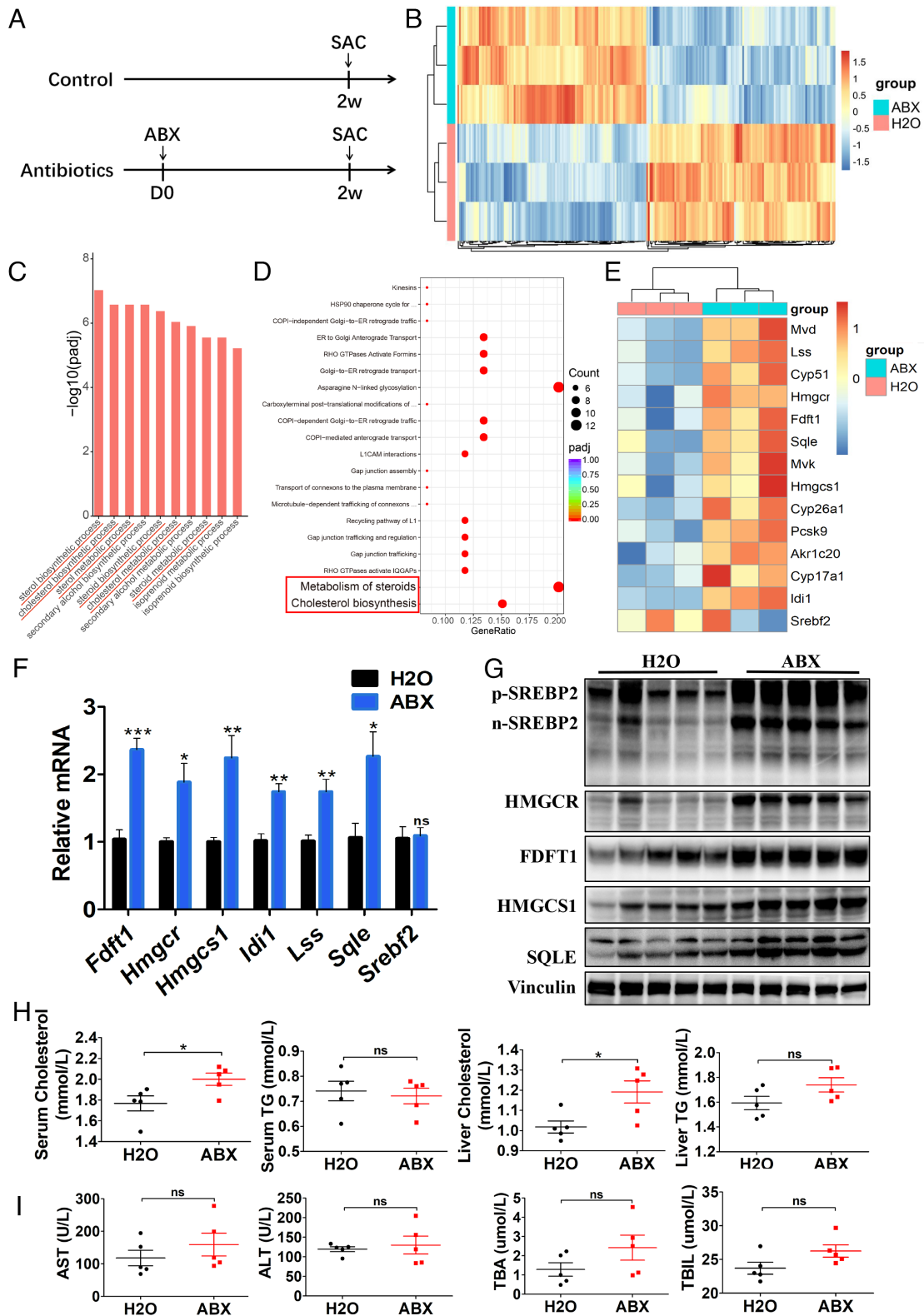
Fig. 3. SREBP2 and downstream cholesterol synthesis-related gene expression increased in mice with gut commensal bacteria depletion. (*A*) Experimental procedure (n = 5 per group). Mice were treated with antibiotics or H$_2$O for 2 wk and killed for further analysis. (*B*) Differentially expressed genes in normal liver tissues from mice in the ABX and H$_2$O groups identified using transcriptome analysis (n = 3 per group). (*C*) Gene Ontology (GO) and (*D*) Reactome pathway enrichment analysis showing the cholesterol metabolism-related processes and pathways, respectively, indicated by red tags. (*E*) Transcriptome analysis of genes involved in cholesterol biosynthesis pathway. (*F*) Gene expression in liver tissues from ABX- or H$_2$O-treated mice was determined by qRT-PCR (n = 5 per group). (*G*) Western blot analysis of liver tissues from ABX- or H$_2$O-treated mice (n = 5 per group). (*H*) Serum and liver cholesterol and triglyceride levels in mice treated with ABX or H$_2$O (n = 5 per group). (*I*) Serum AST, ALT, total bile acid (TBA), and total bilirubin (TBIL) levels in mice treated with ABX or H$_2$O (n = 5 per group). Data were presented as mean ± SEM, *P* values were calculated by Student's *t* test. ns, not significant; *P <0.05; **P <0.01; ***P <0.001.

microenvironment (14). However, in our study, flow cytometry analysis showed that there were no significantly differences in the infiltration of various immune cells either in the liver or spleen of mice treated with ABX (*SI Appendix*, Fig. S6*A*). We also assessed liver tumor initiation in immunodeficient mice treated with ABX. The phenotypic analysis showed that in nude mice, gut flora disequilibrium induced by ABX treatment could also promote HTVi (Ras/Myc)-induced liver cancer formation (*SI Appendix*, Fig. S6 *B* and *C*). And, due to the elevated cholesterol level in the serum and liver in the ABX-treated mice, we explored whether the increased cholesterol accelerated tumor initiation directly. Mice received a high cholesterol diet (HCD, 2% cholesterol) for 2 wk before HTVi (Ras/Myc) (*SI Appendix*, Fig. S6*D*) to elevate the cholesterol level in the blood and liver (*SI Appendix*, Fig. S6*E*). The result showed that mice fed with the HCD did not exhibit an increased tumor burden compared with that in control diet-fed mice (*SI Appendix*, Fig. S6 *F* and *G*). Therefore, we concluded that the change in the cholesterol level was not the key mechanism that drives liver tumor initiation in mice with gut flora disequilibrium.

In tumor initiation, SREBP2 has been reported to act as a potential oncogene in some types of tumors (11, 15, 16). Therefore, we investigated whether increased liver SREBP2 is responsible for the accelerated tumor initiation in mice with gut microbiome depletion. Betulin, an SREBP inhibitor that blocks the SREBP cleavage-activating protein/SREBP pathway, was administered to mice treated with H_2O or ABX (Fig. 4*A*). The validation experiment showed that the hepatic n-SREBP2 level was effectively inhibited by 14 d of betulin treatment in ABX-treated mice (Fig. 4*B*). Betulin treatment failed to reduce the tumor loads in the control mice, but led to a significantly reduced tumor burden in the mice fed with ABX (Fig. 4 *C* and *D*). We then used adeno-associated virus 8 (AAV8) encoding *Srebf2*-RNA interference (AAV8-*Srebf2* KD) to knock down liver *Srebf2* expression. Mice were injected with AAV8-*Srebf2* KD or AAV8-EGFP (AAV8-Vector, as a control), and HTVi (Ras/Myc) was performed 4 wk later (Fig. 4*E*). Validation experiments showed that injection of AAV8-*Srebf2* KD significantly decreased *Srebf2* expression (*SI Appendix*, Fig. S7*A*), and both p-SREBP2 and n-SREBP2 levels were reduced significantly in ABX-treated mice (Fig. 4*F*). The phenotype showed that liver *Srebf2* knockdown recapitulated the rescue effect of betulin treatment that significantly inhibited tumorigenesis in mice treated with ABX (Fig. 4 *G* and *H*). By contrast, we also injected AAV8 expressing *Srebf2* (AAV8-*Srebf2* OE) to overexpress liver SREBP2 in normal mice, and HTVi (Ras/Myc) was performed 4 wk later (Fig. 4*I*). Validation experiments showed significantly increased *Srebf2* expression (*SI Appendix*, Fig. S7*B*) and the levels of both p-SREBP2 and n-SREBP2 in mice with AAV8-*Srebf2* OE injection (Fig. 4*J*). Compared with control mice, SREBP2 overexpression in the liver significantly increased the tumor burden (Fig. 4 *K* and *L*). Thus, we concluded that gut flora disequilibrium-induced SREBP2 overexpression in the liver directly promoted liver tumor initiation.

Gut Flora Disequilibrium Decreased Microbiota-Derived AhR Ligands to Promote Liver Tumorigenesis in Mice. Next, we tried to explore the relationship between gut flora disequilibrium and SREBP2-regulated cholesterol synthesis change in the liver. Tryptophan metabolism in the gut microbiota and the sensor of tryptophan metabolites AhR have been widely studied as an important bridge connecting gut flora disequilibrium and liver disease (17). In general, gut tryptophan can be metabolized by tryptophanase positive bacteria, especially *Escherichia coli* and *Lactobacillus*, to indole and further into more derivatives, such as indole-3-acetic-acid (IAA), which are ligands for AhR

(18). Considering the changed composition of the gut flora caused by ABX treatment, we first explored the effect of gut commensal bacteria depletion on AhR ligands in the gut. Thus, we examined tryptophan and its metabolites using liquid chromatography-tandem mass spectrometry (LC-MS/MS), and 23 metabolites were detected in mouse feces, including an absence of 5-Hydroxytryptophan, indole-3-β-acrylic acid, and tryptamine (below 1 ng/g) in the ABX-treated mice (Fig. 5 *A* and *B*). Indeed, the levels of 10 tryptophan metabolites decreased significantly in the ABX-treated mice, including AhR ligands of IAA, indole-3-carbaldehyde (ICAld), and indole-3-propionic acid (Fig. 5*C*).

AhR has been reported to regulate cholesterol biosynthesis in a dioxin-response element-independent manner and SREBP2 in the liver (19, 20). Therefore, we speculated that depletion of gut commensal bacteria-decreased AhR ligands would affect the SREBP2 level in the liver. To test this hypothesis, the AhR agonist, 6-formylindolo (3,2-b) carbazole (Ficz), was administered to ABX-treated mice and control mice (Fig. 5*D*). The expression of cytochrome p450 family 1 subfamily a member 1 (*Cyp1a1*), the target gene of AhR, was significantly decreased in ABX-treated mice compared to that in control mice, which was also decreased in GF mice compared to that in SPF mice, suggesting an impaired AhR activity in mice with gut flora disequilibrium (Fig. 5*E* and *SI Appendix*, Fig. S8*A*). And, *Cyp1a1* was significantly elevated after Ficz treatment in both control and ABX groups (Fig. 5*E*). Notably, the *Cyp1a1* level was lower in the ABX-treated mice compared with that in the control mice under the same treatment by Ficz. Western blotting results showed that administration of Ficz reduced protein level of both p-SREBP2 and n-SREBP2 significantly, accompanied by a decreased expression of downstream 3-hydroxy-3-methylglutaryl-CoA reductase (HMGCR), the rate-limiting enzyme of cholesterol biosynthesis in ABX-treated mice, but not in the control mice (Fig. 5*F*). Phenotypic analysis showed that the administration of Ficz inhibited tumor burdens significantly in ABX-treated mice, but not in the control mice (Fig. 5 *G* and *H*). We further administrated Ficz in mice transfected with AAV8-*Srebf2* OE to verify this hypothesis. Remarkably, Ficz-induced *Cyp1a1* overexpression in the liver of control mice was significantly higher than that in mice with SREBP2 overexpression, and the protein level of SREBP2 was significantly decreased by Ficz treatment under SREBP2 overexpression condition (*SI Appendix*, Fig. S8 *B–D*). Thus, we concluded that decreased tryptophan metabolism-derived AhR ligands in mice with gut flora disequilibrium attenuated AhR activation, which finally up-regulated SREBP2 to promote tumor initiation in the liver.

Then, we used AhR knockout ($Ahr^{-/-}$) mice to further confirm whether impaired AhR activation directly elevated SREBP2 in mice with gut flora disequilibrium. Both p-SREBP2 and n-SREBP2 levels were elevated significantly in the $Ahr^{-/-}$ mice compared with those in the control mice, accompanied by elevated expression of downstream HMGCR (Fig. 6*A*). Next, we performed HTVi (Ras/Myc) in $Ahr^{-/-}$ and control mice, and the mice were killed 24 d after HTVi for phenotypic analysis. $Ahr^{-/-}$ mice exhibited a significantly increased tumor burden compared with that of the control mice (Fig. 6 *B* and *C*). We next administered Ficz to $Ahr^{-/-}$ mice treated with ABX ($Ahr^{-/-}$-ABX) and control mice treated with ABX (WT-ABX) to further confirm that the effect of Ficz on inhibiting SREBP2 and tumorigenesis could be attributed to AhR activation, rather than other effects of Ficz (Fig. 6*D*). Consistent with our previous observation, both p-SREBP2 and n-SREBP2 levels were repressed by Ficz in WT-ABX mice, accompanied by a decreased expression of HMGCR, while in the $Ahr^{-/-}$-ABX mice, Ficz failed to inhibit liver SREBP2 and downstream HMGCR expression (Fig. 6*E*). Phenotypic analysis also confirmed that Ficz failed to decrease the
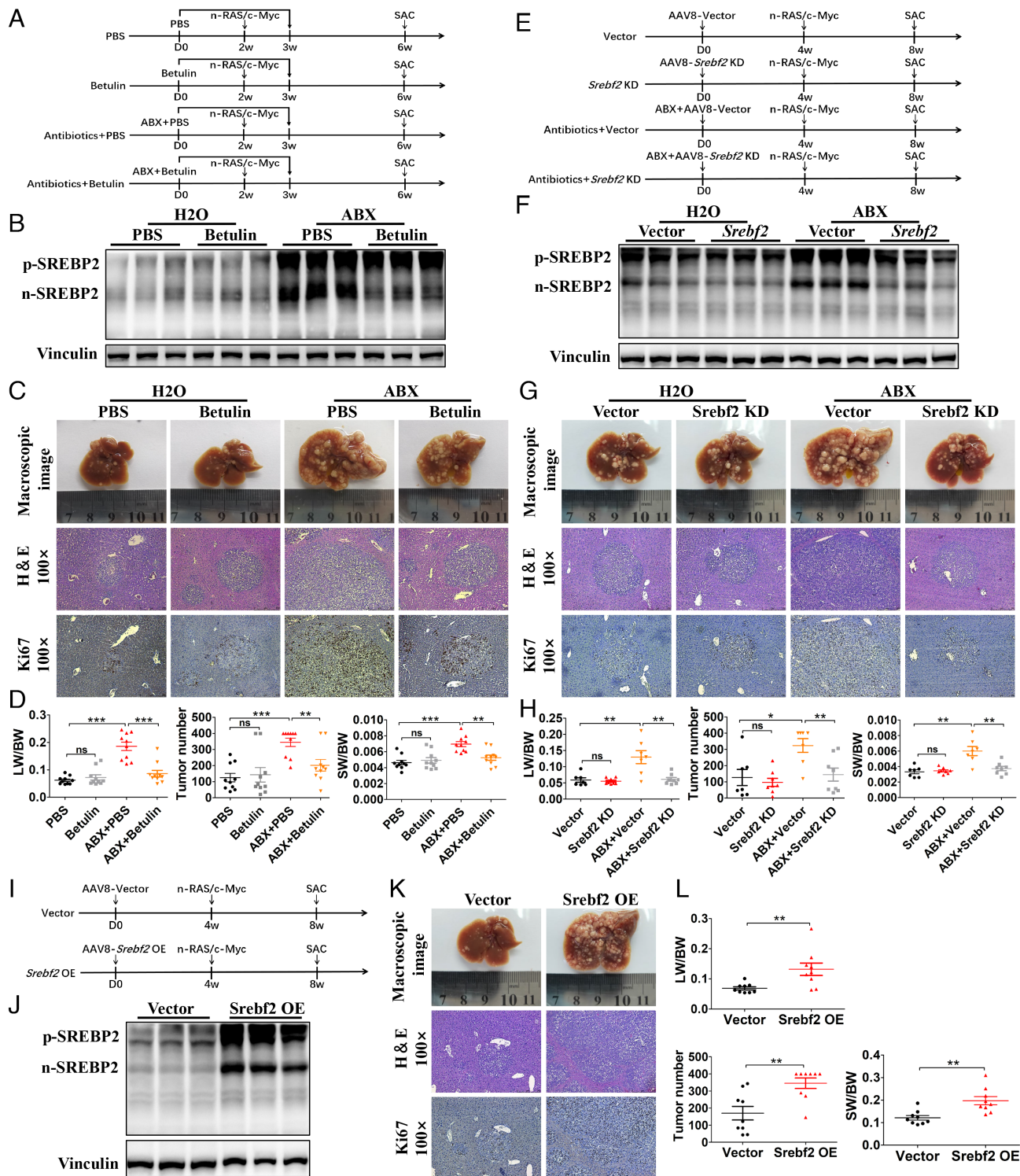
Fig. 4. Elevated liver SREBP2 promoted tumorigenesis in mice with gut commensal bacteria depletion. (*A*) Experimental procedure of betulin administration. (*B*) Western blotting of liver SREBP2 from mice in each group before HTVi (n = 3 per group). (*C*) Representative macroscopic views of livers, H&E staining, and IHC of Ki67 in mouse HCCs. (*D*) The LW/BW ratio, tumor number, and the SW/BW ratio of each group (n = 10 per group). (*E*) Experimental procedure of AAV8-mediated *Srebf2* knockdown. (*F*) The AAV8-*Srebf2* KD-mediated knockdown of liver SREBP2 was analyzed using Western blotting before HTVi (n = 3 per group). (*G*) Representative macroscopic views of livers, H&E staining, and IHC of Ki67 in mouse HCCs. (*H*) The LW/BW ratio, tumor number, and the SW/BW ratio of AAV8-vector or AAV8-*Srebf2* KD-transfected mice fed with ABX or H₂O (Vector, n = 7; *Srebf2* KD, n = 8; ABX+Vector, n = 7; ABX+*Srebf2* KD, n = 8). (*I*) Mice were transfected with AAV8-vector or AAV8-*Srebf2* OE, and HTVi (Ras/Myc) was performed 4 wk after AAV transfection. (*J*) The AAV-mediated overexpression of liver SREBP2 was analyzed using Western blotting before HTVi (n = 3 per group). (*K*) Mice transfected with the AAV8-vector or AAV8-*Srebf2* OE were killed 4 wk after HTVi, shown are representative macroscopic views of the livers, H&E staining, and IHC of Ki67 in mouse HCCs. (*L*) The LW/BW ratio, tumor number, and the SW/BW ratio of AAV8-vector or AAV8-*Srebf2* OE mice (n = 9 per group). Data were presented as mean ± SEM, *P* values were calculated by Student's *t* test. ns, not significant; **P <0.01; ***P <0.001.

tumor burden in $Ahr^{-/-}$-ABX mice (Fig. 6 *F* and *G*). Overall, these results further confirmed that AhR inhibited liver SREBP2 levels and attenuated tumorigenesis in mice.

Treatment with *Lactobacillus Reuteri* Attenuated Liver Tumor Initiation in Mice with Gut Flora Disequilibrium. Next, we investigated whether supplementation of tryptophanase-positive
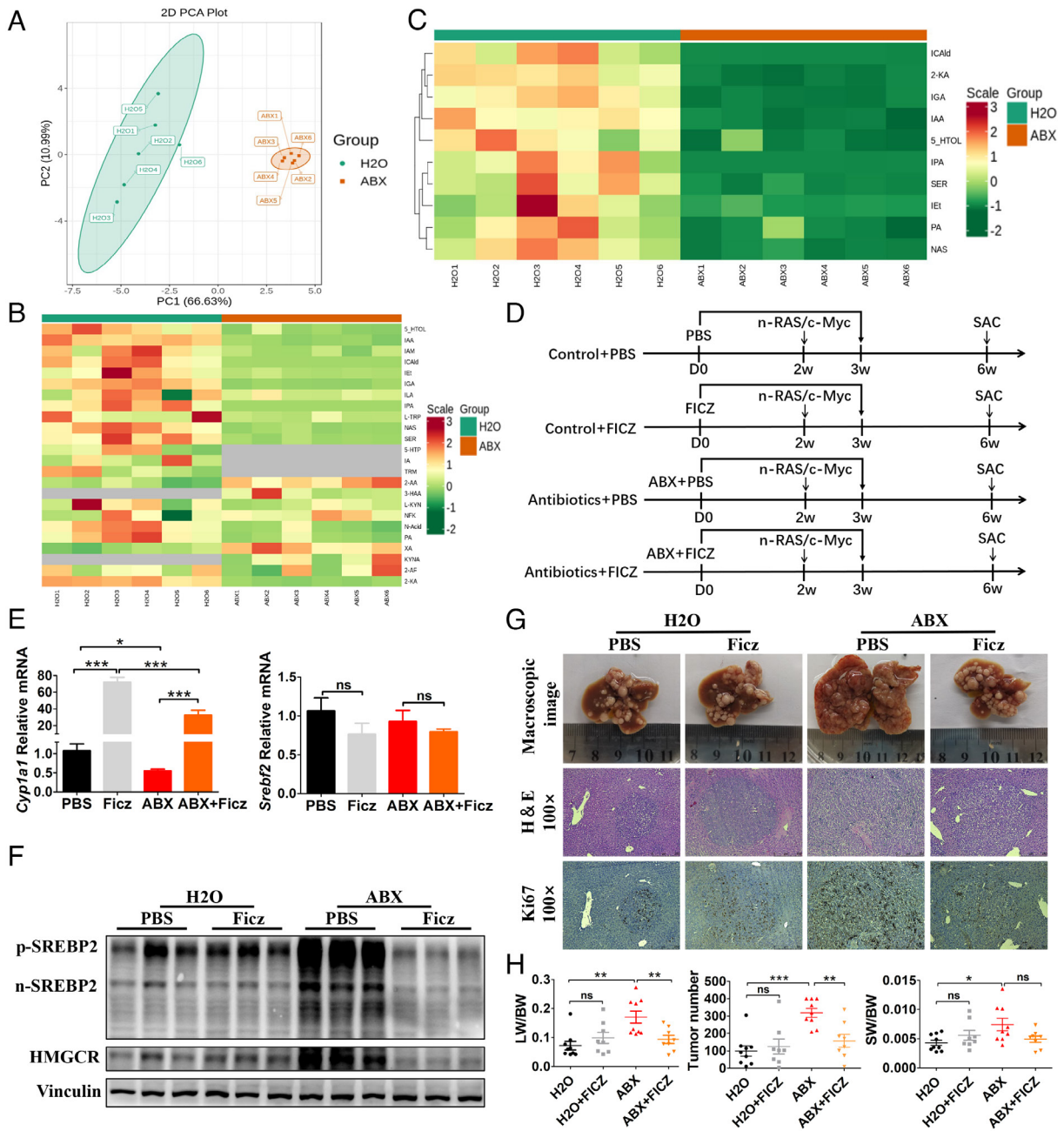
Fig. 5. Gut flora disequilibrium decreased microbiota-derived AhR ligands to promote liver tumorigenesis in mice by up-regulating SREBP2. (*A*) PCA analysis of fecal tryptophan metabolic data from ABX- or H$_2$O-fed mice (n = 6 per group). (*B*) Heatmap showing that 24 tryptophan metabolites were detected in mice with ABX or H$_2$O. (*C*) Heatmap showing decreased microbiota-derived AhR ligands in mice treated with ABX compared to mice treated with H$_2$O. (*D*) Experimental procedure of Ficz administration. (*E*) Liver mRNA levels of *Cyp1a1* and *Srebf2* were determined by qRT-PCR before HTVi (n = 6 per group). (*F*) Liver levels of SREBP2 and HMGCR in each group before HTVi (n = 3 per group). (*G*) Representative macroscopic views of livers, H&E staining, and IHC of Ki67 in mouse HCCs. (*H*) The LW/BW ratio, tumor number, and the SW/BW ratio of each group (PBS, n = 9; Ficz, n = 8; ABX+PBS, n = 9; ABX+Ficz, n = 8). Data were presented as mean ± SEM, *P* values were calculated by Student's *t* test. ns, not significant; *P <0.05; **P <0.01; ***P <0.001.

bacteria could reduce liver SREBP2 and tumor initiation in mice with gut flora disequilibrium. According to our 16S rRNA sequencing results, *Lactobacillus* represented the second largest proportion of the bacteria that were significantly reduced in ABX-treated mice (*SI Appendix*, Fig. S1*C*). And, it has been reported that *L. reuteri* has strong ability to metabolize tryptophan and exhibits high AhR ligand production (17, 21). Therefore, *L. reuteri* bacteria or lactic acid bacterial culture (MRS) medium was administrated every other day after ABX cocktail treatment for 13 d, and 1 d later, HTVi (Ras/Myc) was performed (Fig. 7*A*). The feces of each group were collected before HTVi, and fecal tryptophan and its metabolites were detected using LC-MS/MS analysis. Principal

component analysis (PCA) showed that administration of *L. reuteri* in mice with gut flora disequilibrium produced similar tryptophan metabolites compared with those in the control mice (Fig. 7*B*). All the detected tryptophan metabolites were identified and six metabolites increased significantly after administration of *L. reuteri* in mice with gut flora disequilibrium, among which IAA and ICAld were ligands for AhR (Fig. 7 *C* and *D*). In the liver, administration of *L. reuteri* significantly reduced the protein levels of both p-SREBP2 and n-SREBP2 in mice with gut flora disequilibrium (Fig. 7*E*). Mice were killed 4 wk after HTVi (Ras/Myc), and phenotypic analysis showed that administration of *L. reuteri* significantly attenuated tumor formation in mice
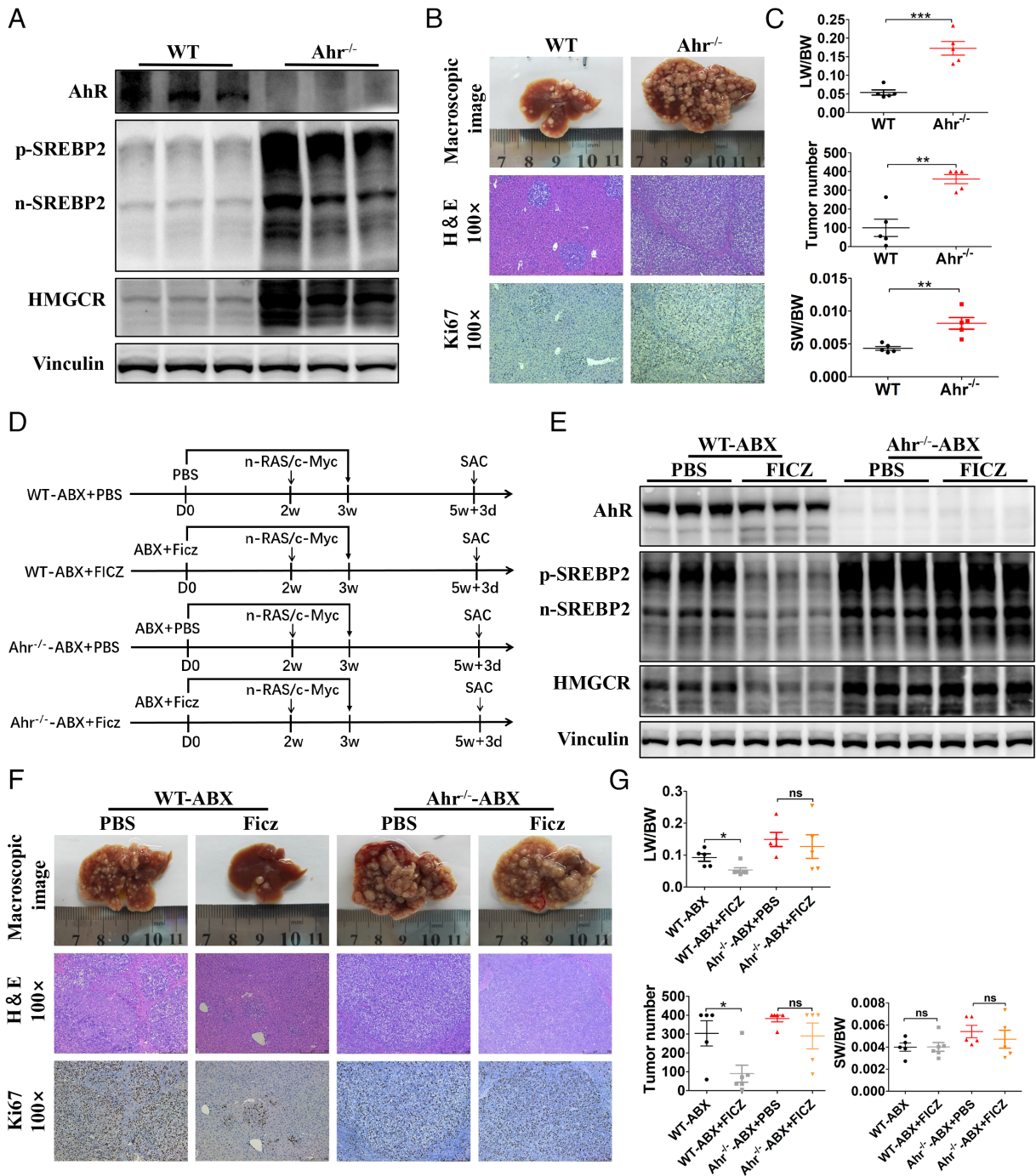
Fig. 6. *Ahr*^{−/−} mice exhibited increased liver SREBP2 expression and accelerated tumorigenesis. (*A*) The levels of SREBP2 and HMGCR were analyzed by Western blotting in livers from WT and *Ahr*^{−/−} mice (n = 3 per group). (*B*) WT or *Ahr*^{−/−} mice were transfected with Ras/Myc by HTVi and killed 24 d later. Representative macroscopic views of livers, H&E staining, and IHC of Ki67 in mouse HCCs. (*C*) The LW/BW ratio, tumor number, and the SW/BW ratio of each group (WT n = 5; *Ahr*^{−/−} n = 5). (*D*) Experimental procedure. WT or *Ahr*^{−/−} mice with ABX treatment were given PBS or Ficz by intraperitoneal injection once daily for 21 consecutive days. Mice were transfected with Ras/Myc by HTVi 2 wk after PBS or Ficz treatment and were killed 24 d after HTVi. (*E*) Levels of AhR, SREBP2, and HMGCR were analyzed using Western blotting in livers of WT and *Ahr*^{−/−} mice. (*F*) Representative macroscopic views of livers, H&E staining, and IHC of Ki67 in mouse HCCs. (*G*) The LW/BW ratio, tumor number, and the SW/BW ratio of each group (WT-ABX + PBS, n = 5; WT-ABX + Ficz, n = 6; *Ahr*^{−/−}-ABX + PBS, n = 5; *Ahr*^{−/−}-ABX + Ficz, n = 5). Data were presented as mean ± SEM, *P* values were calculated by Student's *t* test. ns, not significant; *P* <0.05; **P* <0.01; ***P* <0.001.

with gut flora disequilibrium (Fig. 7*F*). In mice with gut flora disequilibrium, tumor burdens were significantly reduced after *L. reuteri* supplementation (Fig. 7*G*). We further administered *L. reuteri* to *Ahr*^{−/−}-ABX and WT-ABX mice to confirm that the effect of *L. reuteri* on inhibiting SREBP2 and tumorigenesis was attributed to AhR activation. In *Ahr*^{−/−}-ABX mice, *L. reuteri* failed to inhibit liver SREBP2 expression and tumor initiation (*SI Appendix*, Fig. S9 *A–D*). Overall, these results suggested that

supplementation with *L. reuteri* increased microbiota-derived AhR ligands, which was similar to the effect of Ficz treatment, i.e., it decreased SREBP2 and tumor initiation in mice with gut flora disequilibrium.

Insufficient Fecal IAA Level Was Accompanied with Tumorous Reduced AhR Activity and Increased SREBP2 Expression in Patients with HCC. We next investigated the relevance of these
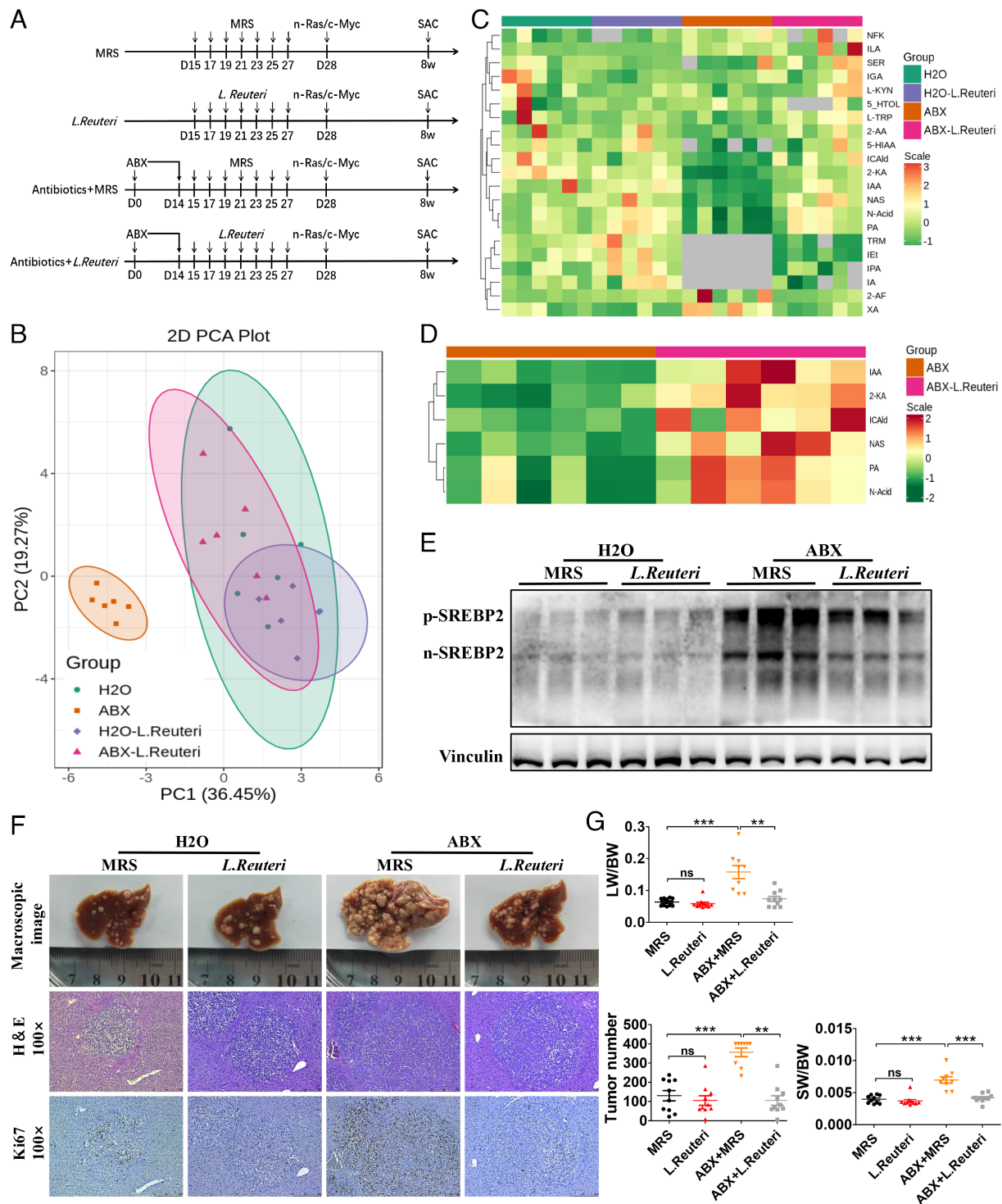
Fig. 7. *L. reuteri* supplementation increased microbiota-derived AhR ligands and suppressed tumorigenesis in mice with gut flora disequilibrium. (*A*) Experimental procedure of *L. reuteri* administration. (*B*) PCA of fecal tryptophan metabolic data of the mice from the four groups before HTVi (n = 6 per group). (*C*) Heatmap showing that 20 tryptophan metabolites were detected in mouse feces. (*D*) Increased microbiota-derived AhR ligands in ABX + *L. Reuteri* mice compared with that in ABX mice. (*E*) The liver level of SREBP2 was analyzed using Western blotting before HTVi (n = 3 per group). (*F*) Representative macroscopic views of livers, H&E staining, and IHC of Ki67 in mouse HCCs. (*G*) The LW/BW ratio, tumor number, and the SW/BW ratio of each group (MRS, n = 10; *L. Reuteri*, n = 10; ABX + MRS, n = 9; ABX + *L. Reuteri*, n = 10). Data were presented as mean ± SEM, *P* values were calculated by Student's *t* test. ns, not significant; ***P* < 0.01; ****P* < 0.001.

findings in human disease; the fecal samples of HCC patients and healthy subjects were used for detecting tryptophan metabolites and microbiome 16S rRNA sequencing. Five tryptophan metabolites were changed significantly in HCC patients compared to those in healthy subjects, among which IAA and ICAld were AhR ligands. The level of IAA was decreased and the level of ICAld was increased in HCC patients. Notably, the average concentrations of IAA in healthy

subjects vs. HCC patients were 2022.34 ng/g vs. 1124.50 ng/g, and the average concentrations of ICAld in healthy subjects vs. HCC patients were 66.43 ng/g vs. 128.50 ng/g, which was much lower than that of IAA (*SI Appendix*, Fig. S10 *A* and *B*). Besides, it has been reported that IAA is the dominant AhR activator but not ICAld in mice and humans (22). 16S rRNA sequencing showed that at phylum level, the relative abundance of *Firmicutes*

was decreased and *Proteobacteria* was increased in HCC patients compared to that in healthy subjects. At genus level, the *Blautia* genus represented the significantly decreased genus in HCC group (*SI Appendix*, Fig. S10 *C* and *D*). We further examined the *Cyp1a1* expression in HCC tissues and matched adjacent nontumor tissues, and the results showed that *Cyp1a1* was significantly decreased in HCC tissues (*SI Appendix*, Fig. S10*E*). We also observed a positive correlation between fecal IAA level and *Cyp1a1* expression in patients with HCC (*SI Appendix*, Fig. S10*F*). And, increased SREBP2 expression was observed in HCC tissues compared to that in matched adjacent nontumor tissues (*SI Appendix*, Fig. S10*G*). Overall, these results showed that in HCC patients, reduced fecal IAA was correlated with impaired AhR activation and increased SREBP2 expression in HCC tissues.

Discussion

Liver cancer is one of the most common primary tumors worldwide, with increasing rates of morbidity and mortality (23). An increasing body of evidence shows that liver cancer is associated with changes in gut microbiota abundance, composition, and barrier function, which are related to the participation of metabolites from microbes in gut (24). In this study, we found that a balanced gut microbiota played an important role in preventing liver tumor initiation. Specifically, gut flora disequilibrium induced using antibiotics or using GF mice elevated SREBP2 levels in the liver, which accelerated liver tumor initiation. More importantly, we found that microbiota-derived AhR ligands were markedly decreased in mice with gut flora disequilibrium. Moreover, *Ahr*$^{-/-}$ mice showed up-regulated SREBP2 levels in the liver and showed enhanced liver tumor initiation. Furthermore, we used Ficz to directly activate AhR or the bacteria *L. reuteri*, which increased intestinal AhR ligands to activate AhR, which both reversed the abnormal liver SREBP2 elevation and inhibited liver tumorigenesis in mice with gut flora disequilibrium (*SI Appendix*, Fig. S11).

Studies have revealed the crucial influence of the gut microbiome in liver cancer. It was reported that gut microbiome-derived LPS is required for liver tumor promotion, which depended on a TLR4-mediated increase in proliferation, the expression of the hepatomitogen, epiregulin, and prevention of apoptosis in liver cells (4). In addition, gut microbiome-mediated primary-to-secondary bile acid conversion controlled natural killer T (NKT) cell accumulation by CXCL16 expression and protected against liver tumor progression (5). These studies demonstrated that depletion of the gut microbiome inhibited liver tumor progression, which, however, played an opposite role in tumor initiation in our study. By using hydrodynamic transfection-induced liver cancer models, we explored the roles of the gut microbiome in both liver tumor initiation and progression. After liver tumors were developed, depletion of gut microbiome did not accelerate or inhibit liver cancer in mice, suggesting the different mechanisms by which gut microbiota affects tumor initiation and development. In diethyl-nitrosamine (DEN)-induced liver cancer in rats, induction of enteric dysbacteriosis or intestinal inflammation by penicillin promoted tumor formation, which was associated with the translocation of endotoxin and activation of damage-associated molecular patterns (25). In other types of cancer, the relationship between the gut microbiota and tumor initiation has rarely been studied. In the initiation of colitis-associated cancer, the gut microbiota facilitates tumorigenesis by generating a precancerous inflammatory milieu (26). In melanoma, it was reported that antibiotic-induced gut microbiota disequilibrium also promoted tumor initiation by affecting antigen-presenting cell development in mice (27).

Recent studies have revealed the effect of gut microbiome in regulating cholesterol synthesis in the liver, which directly affects liver homeostasis and causes liver disease (9, 28). In this study, we detected the abnormal activation of the mevalonate pathway in the liver with gut flora disequilibrium, and the expression of SREBP2 was responsible for promoting liver tumor initiation. A previous study demonstrated that loss of p53 induced liver tumorigenesis via activation of SREBP2 and the mevalonate pathway (11). Several studies also revealed that SREBP2 is aberrantly activated in other types of cancers, including melanoma, prostate cancer, and colorectal cancer (29–31). In melanoma, SREBP2-driven iron homeostatic pathways, which include transcription of the iron carrier transferrin to reduce intracellular iron pools, reactive oxygen species, and lipid peroxidation, contribute to cancer progression, drug resistance, and metastasis (31). In our study, gut flora disequilibrium-induced liver SREBP2 overexpression was accompanied by enhanced cholesterol synthesis, which, however, does not seem to participate directly in liver tumor initiation, as assessed using an oral cholesterol test. In more detail, the transcriptional level of *Srebf2* was unchanged; however, the levels of p-SREBP2 and n-SREBP2 were elevated significantly, suggesting that SREBP2 was posttranslationally modified to directly regulate liver tumorigenesis. Therefore, the underlying mechanisms by which elevated SREBP2 promotes liver tumorigenesis remain to be further elucidated.

This study addressed the importance of microbiota-derived tryptophan metabolites and AhR activation in modulating liver tumorigenesis. Tryptophan metabolism has been strongly linked to cancer pathogenesis, and most of the studies revealed that tryptophan metabolites are accumulated by the overexpression of tryptophan-degrading enzymes, including indoleamine 2,3-dioxygenase 1 (IDO1), in tumor cells, leading to suppression of the tumor immune response (32, 33). Few studies have focused on the effect of tryptophan metabolism associated with the microbiota in cancers. In colorectal cancer, alteration of fecal tryptophan metabolism mediated by the microbiota is associated with intestinal barrier function and is involved in its pathogenesis, which might be exploited to develop novel therapeutic approaches (34, 35). In the gut, tryptophan is metabolized by gut bacteria, especially *E. coli* and *Lactobacillus*, which express tryptophanase to produce indole and its derivatives, which are the most important endogenous AhR ligands (17, 21). One of the tryptophan metabolites, IAA, was reported to have protective effects on DEN-induced liver tumorigenesis (36). AhR has been reported to function as a tumor suppressor by regulating cell proliferation, DNA damage, and inflammatory cytokine expression (37). Conversely, Hezaveh et al. proved a tumor-promotive function of microbial-derived AhR signaling in the progression of pancreatic ductal adenocarcinoma (38). These evidences suggested the complex functions of AhR signaling in different tumor types and different tumor stages. In our study, gut flora disequilibrium led to inhibited AhR function, which could be reactivated by supplementation with *L. reuteri*, by increasing AhR ligands, or by the AhR agonist Ficz, making it clinically possible to prevent liver tumor initiation through AhR activation.

We found that the fecal IAA was insufficient in HCC patients and further confirmed that the AhR activation was impaired in HCC tissues. The proportion of potentially pathogenic bacteria *Proteobacteria* which has been proposed to be a hallmark of gut flora disequilibrium was significantly increased in HCC patients (39). Meanwhile, the proportion of *Firmicutes* which contains most of the probiotic bacteria was significantly decreased in HCC patients. And, the reduced IAA was most likely due to the altered intestinal microbiota in HCC patients. However, the gut

microbiota composition was quite different between humans and mice; for example, the proportion of *Lactobacillus* in healthy humans is much less than that in SPF mice (0.19% vs. 23.5%) and the proportion of *Blautia* in healthy humans is much more than that in SPF mice (8.14% vs. 0.09%). We found that the proportion of *Lactobacillus* showed no significant difference between HCC patients and healthy subjects, while the proportion of *Blautia* was significantly decreased in HCC patients. A previous study suggested that *Blautia* was able to metabolize tryptophan, and we speculated that reduced proportion of *Blautia* in HCC patients led to reduced IAA and AhR activation (40). This suggested that the species of gut microflora that are responsible for metabolism of tryptophan in mice may differ substantially from that in humans. Moreover, it is difficult to obtain the human samples during the initiation of HCC; considering the different roles of gut flora in liver tumor initiation and progression, these results from human subjects should be interpreted with caution.

This study revealed the inhibitory effect of AhR on SREBP2 in liver cancer. However, the underlying mechanism remains obscure. Only one previous study proved that in vitro, AhR is an adaptor protein of the ubiquitin ligase complex and can degrade SREBP2 through the ubiquitin–proteasomal pathway in a calcium-dependent manner (19). In our study, we found that AhR activation strongly decreased both p-SREBP2 and n-SREBP2; however, it did not affect the mRNA level of *Srefb2* (Fig. 5*E*), suggesting that AhR inhibits SREBP2 function by posttranslational modification. In addition, AhR activation by Ficz significantly inhibited SREBP2, accompanied by downstream expression of HMGCR, but not in the control mice (Fig. 5*F*), suggesting that AhR activation might function only when SREBP2 is abnormally overexpressed. Indeed, once SREBP2 was overexpressed, AhR activation by Ficz showed increased SREBP2 inhibitory activity (*SI Appendix*, Fig. S8). Therefore, the underlying mechanism of AhR-SREBP2 signaling pathway requires further study.

In recent years, FMT-based microbiological therapy has become a hot spot of cancer research, which also has led to the development of preclinical and clinical manipulations in cancer management (41). In a clinical study, FMT was proven to promote an antitumor response in patients with immunotherapy-refractory melanoma (42). Increasing evidence indicates the potential therapeutic value of FMT in liver cancer (43). However, the "healthy" microbiome is hard to define well from the gut microbiota community. Among them, *Lactobacillus* is one of the bacterial genera that has valuable probiotic properties. Here, we identified that FMT with *L. reuteri* decelerated liver cancer initiation in mice with gut flora disequilibrium. A previous study showed that *L. reuteri* could stimulate the body to produce anticancer cytokines, including tumor necrosis factor-alpha and interferon-gamma to inhibit the migration and colonization of melanoma (44). In inflammation-associated colorectal cancer, the administration of decarboxylase-positive *L. reuteri* produced histamine, which decreased the number and size of colon tumors by reducing the amounts of proinflammatory cancer-associated cytokines and keratinocyte chemoattractants (45). In the present study, *L. reuteri* was proven to prevent liver tumor initiation through tryptophan metabolism, revealing its multiple potentials in tumor prevention.

Exploring the mechanisms of tumor initiation has significant clinical benefits for the early detection and intervention of cancer. Overall, we identified the role of tryptophan metabolites derived from the gut microbiota in regulating SREBP2 expression through AhR signaling in the liver, which is critical to preventing liver tumor initiation. Our study provides insights into the prevention of liver tumorigenesis and might contribute to the development of strategies for liver cancer prevention.

Materials and Methods

Mice and Tumor Models. Male C57BL/6J mice and Balb/c nude mice were purchased from GemPharmatech, and mice aged 7 to 9 wk were used for the experiments. $Ahr^{-/-}$ mice with a C57BL/6 background were purchased from Shanghai Model Organisms Center Inc. The above mice were housed and bred in an SPF animal facility at the Experimental Animal Center of the First Affiliated Hospital, School of Medicine, Zhejing University, on a 12-h light–dark cycle. GF C57BL/6 mice were purchased from Cyagen Biosciences Inc. and maintained in GF isolators. Mouse primary liver tumors were induced by HTVi of oncogenes including PT3-EF1a-C-Myc and PT/Caggs-NRas-V12 (Ras/Myc), PT3-EF1a-c-Met and PT3-EF1a-N90-β-catenin (MET/CAT), or Pt3-EF1a-myrAKT-HA and PT3-EF1a-FLAG-YAP S127A (YAP/AKT) combined together with the sleeping beauty transposase, pCMV-SB11, which were obtained from Addgene (www.addgene.com), and these oncogene plasmids were also approved by the depositor Xin Chen (Xin.Chen@ucsf.edu) at the University of California, San Francisco. The plasmid of pT3-EF1a-N90-β-catenin was a gift from Dr. Bin Zhao (binzhao@zju.edu.cn) at Zhejiang University, School of Medicine. Plasmid DNAs were diluted in phosphate-buffered saline (PBS) and injected at 0.1 mL/g body weight of mice through the tail vein in 7 to 8 s. In the experiments including GF mice, the mice were injected with Ras/Myc at 0.07 mL/g body weight through the tail vein in 7 to 8 s. The Hep1-6 cell line was purchased from the American Type Culture Collection (ATCC). The KPC cell line, derived from spontaneous tumors in a Kras$^{LSL-G12D}$; Trp$^{53LSL-R172H}$; Pdx1-Cre mouse model, was a gift from Raghu Kalluri at the MD Anderson Cancer Center of Houston, Texas. 3×10^5 Hep1-6 tumor cells were administered by subcutaneous or tail vein injection, and 1×10^6 KPC tumor cells were administered by intrasplenic injection. The mice were monitored by abdominal palpation and killed when the abdomen was enlarged in some of the mice; at this time point, the mice did not present weakness, jaundice, or any other abnormal symptoms in physical and mental status. All experiments were approved by the Ethics Committee of the First Affiliated Hospital, School of Medicine, Zhejiang University.

Drug and AAV Administration. Antibiotic-treated mice received a cocktail of three antibiotics: vancomycin (500 mg/L; Sigma, catalog # V2002), ampicillin (1 g/L; Sigma, catalog # A9518), and neomycin (1 g/L; Sigma, catalog # N6386) in drinking water, which was replaced every other day to maintain sterility. To inhibit SREBP2, the mice were treated by oral gavage of betulin (2 mg/mouse; Sigma, catalog # B9757) or vehicle (PBS) once per day for 21 d. To activate AhR, the mice were injected intraperitoneally with Ficz (1 μg/mouse; Sigma, catalog # SML1489) or vehicle (0.4% dimethyl sulfoxide (DMSO) in PBS) once per day for 21 d. For *Srefb2* knockdown in the liver, recombinant AAV8 vectors containing *Srefb2*-RNA interference or Enhanced Green Fluorescent Protein (EGFP) with an ApoE/hAATp promoter (AAV8-*Srefb2* KD, AAV8-EGFP) were generated by Genechem Co., Ltd. For *Srefb2* overexpression in the liver, AAV8 vectors containing *Srefb2* with a ApoE/hAATp promoter (AAV8-*Srefb2* OE) or empty vector (AAV8-vector) were generated by Genechem Co., Ltd. AAV8-*Srefb2* KD, AAV8-EGFP, AAV8-*Srefb2* OE, or AAV8-vector was diluted in 200 μL of PBS (1×10^{11} v.g/mouse) and delivered via tail vein injection. Four weeks after AAV8 delivery, *Srefb2* knockdown or overexpression was verified by qRT-PCR and Western blotting.

Fecal Microbiota Transplantation and *L. Reuteri* Administration. Fresh stool samples from healthy C57BL/6J mice (8-wk-old, male) were mixed and suspended using PBS (200 mg/mL). The suspension was filtered through 70 μm strainers and then used for FMT. GF and control SPF mice received FMT or PBS by gavage (200 μL/mouse) every other day for 14 d and then HTVi was performed. For the supplementation of *L. reuteri* (ATCC 53608), *L. reuteri* was grown anaerobically in MRS medium at 37 °C for 16 h and reached a concentration of 10^7 CFU/mL bacteria liquid, which was calculated via the plate counting method. Then, the bacterial culture was centrifuged at $3,500 \times g$ for 10 min, the supernatant was discarded, and the pellet was resuspended for gavage (10^9 CFU/mouse). The mice were pretreated with the ABX cocktail for 14 d to deplete the gut commensal bacteria. Then, ABX pretreated and control mice received *L. reuteri* bacteria or MRS by gavage (200 μL/mouse) once a day for 14 d, followed by HTVi.

Statistical Analysis. Statistical analysis was performed using GraphPad Prism 5.0 (GraphPad Inc.) and SPSS 19.0 (IBM Corp.). In all figures, the data were represented as the mean ± SEM. Comparisons between two independent groups or paired groups were performed using two-tailed unpaired Student's *t* test or paired *t* test, $P < 0.05$ was considered statistically significant (*$P < 0.05$, **$P < 0.01$,

***$P < 0.001$), and "ns" indicates no significance. Survival curves were plotted using Kaplan–Meier analysis and compared using the log-rank test, and $P < 0.05$ was considered statistically significant.

Data, Materials, and Software Availability. All study data are included in the article and/or *SI Appendix*.

Author affiliations: [a]Zhejiang Provincial Key Laboratory of Pancreatic Disease, The First Affiliated Hospital, School of Medicine, Zhejiang University, Hangzhou, Zhejiang 310003, China; [b]Zhejiang Clinical Research Center of Hepatobiliary and Pancreatic Disease, Hangzhou, Zhejiang 310009, China; [c]Zhejiang University Cancer Center, Hangzhou, Zhejiang 310014, China; and [d]Department of Hepatobiliary and Pancreatic Surgery, The First Affiliated Hospital, School of Medicine, Zhejiang University, Hangzhou, Zhejiang 310003, China

1. A. Villanueva, Hepatocellular carcinoma. *N. Engl. J. Med.* **380**, 1450–1462 (2019).
2. D. Hanahan, Hallmarks of cancer: New dimensions. *Cancer Discov.* **12**, 31–46 (2022).
3. L. X. Yu, R. F. Schwabe, The gut microbiome and liver cancer: Mechanisms and clinical translation. *Nat. Rev. Gastroenterol. Hepatol.* **14**, 527–539 (2017).
4. D. H. Dapito *et al.*, Promotion of hepatocellular carcinoma by the intestinal microbiota and TLR4. *Cancer Cell* **21**, 504–51 (2012).
5. C. Ma *et al.*, Gut microbiome-mediated bile acid metabolism regulates liver cancer via NKT cells. *Science* **360**, 5931 (2018).
6. T. M. Loo *et al.*, Gut microbiota promotes obesity-associated liver cancer through PGE2-mediated suppression of antitumor immunity. *Cancer Discov.* **7**, 522–538 (2017).
7. X. Liu, Y. Chen, S. Zhang, L. Dong, Gut microbiota-mediated immunomodulation in tumor. *J. Exp. Clin. Cancer Res.* **40**, 221 (2021).
8. S. Rabot *et al.*, Germ-free C57BL/6J mice are resistant to high-fat-diet-induced insulin resistance and have altered cholesterol metabolism. *FASEB J.* **24**, 4948–4959 (2010).
9. T. Le Roy *et al.*, The intestinal microbiota regulates host cholesterol homeostasis. *BMC Biol.* **17**, 94 (2019).
10. P. J. Mullen, R. Yu, J. Longo, M. C. Archer, L. Z. Penn, The interplay between cell signalling and the mevalonate pathway in cancer. *Nat. Rev. Cancer* **16**, 718–731 (2016).
11. S. H. Moon *et al.*, p53 represses the mevalonate pathway to mediate tumor suppression. *Cell* **176**, 564580.e519 (2019).
12. X. Zhang *et al.*, Dietary cholesterol drives fatty liver-associated liver cancer by modulating gut microbiota and metabolites. *Gut* **70**, 761–774 (2021).
13. L. Wen *et al.*, An efficient combination immunotherapy for primary liver cancer by harmonized activation of innate and adaptive immunity in mice. *Hepatology* **69**, 2518–2532 (2019).
14. B. Huang, B. L. Song, C. Xu, Cholesterol metabolism in cancer: Mechanisms and therapeutic opportunities. *Nat. Metab.* **2**, 132–141 (2020).
15. L. Che *et al.*, Cholesterol biosynthesis supports the growth of hepatocarcinoma lesions depleted of fatty acid synthase in mice and humans. *Gut* **69**, 177–186 (2020).
16. B. Liang *et al.*, ASPP2 inhibits tumor growth by repressing the mevalonate pathway in hepatocellular carcinoma. *Cell Death Dis.* **10**, 830 (2019).
17. J. M. Natividad *et al.*, Impaired aryl hydrocarbon receptor ligand production by the gut microbiota is a key factor in metabolic syndrome. *Cell Metab.* **28**, 737–749.e734 (2018).
18. W. R. Wikoff *et al.*, Metabolomics analysis reveals large effects of gut microflora on mammalian blood metabolites. *Proc. Natl. Acad. Sci. U.S.A.* **106**, 3698–3703 (2009).
19. G. E. Muku *et al.*, Selective Ah receptor modulators attenuate NPC1L1-mediated cholesterol uptake through repression of SREBP-2 transcriptional activity. *Lab. Invest.* **100**, 250–264 (2020).
20. R. Tanos *et al.*, Aryl hydrocarbon receptor regulates the cholesterol biosynthetic pathway in a dioxin response element-independent manner. *Hepatology* **55**, 1994–2004 (2012).
21. B. Lamas *et al.*, CARD9 impacts colitis by altering gut microbiota metabolism of tryptophan into aryl hydrocarbon receptor ligands. *Nat. Med.* **22**, 598–605 (2016).
22. F. Dong *et al.*, Intestinal microbiota-derived tryptophan metabolites are predictive of Ah receptor activity. *Gut Microbes* **12**, 1–24 (2020).
23. D. Sia, A. Villanueva, S. L. Friedman, J. M. Llovet, Liver cancer cell of origin, molecular class, and effects on patient prognosis. *Gastroenterology* **152**, 745–761 (2017).
24. M. Moreno-Gonzalez, N. Beraza, The role of the microbiome in liver cancer. *Cancers (Basel)* **13**, 2330 (2021).
25. H. L. Zhang *et al.*, Profound impact of gut homeostasis on chemically-induced pro-tumorigenic inflammation and hepatocarcinogenesis in rats. *J. Hepatol.* **57**, 803–812 (2012).
26. Y. Yang *et al.*, Cross-talk between the gut microbiota and monocyte-like macrophages mediates an inflammatory response to promote colitis-associated tumourigenesis. *Gut* **70**, 1495–1506 (2020).
27. C. Xu *et al.*, Antibiotics-induced gut microbiota dysbiosis promotes tumor initiation via affecting APC-Th1 development in mice. *Biochem. Biophys. Res. Commun.* **488**, 418–424 (2017).
28. R. Caesar, H. Nygren, M. Oresic, F. Backhed, Interaction between dietary lipids and gut microbiota regulates hepatic cholesterol metabolism. *J. Lipid. Res.* **57**, 474–481 (2016).
29. X. Hong *et al.*, The lipogenic regulator SREBP2 induces transferrin in circulating melanoma cells and suppresses ferroptosis. *Cancer Discov.* **11**, 678–695 (2021).
30. M. Chen *et al.*, An aberrant SREBP-dependent lipogenic program promotes metastatic prostate cancer. *Nat. Genet.* **50**, 206–218 (2018).
31. B. Sharma *et al.*, Clinical relevance of cholesterol homeostasis genes in colorectal cancer. *Biochim. Biophys. Acta Mol. Cell Biol. Lipids* **1864**, 1314–1327 (2019).
32. M. Platten, E. A. A. Nollen, U. F. Rohrig, F. Fallarino, C. A. Opitz, Tryptophan metabolism as a common therapeutic target in cancer, neurodegeneration and beyond. *Nat. Rev. Drug Discov.* **18**, 379–401 (2019).
33. I. Theate *et al.*, Extensive profiling of the expression of the indoleamine 2,3-dioxygenase 1 protein in normal and tumoral human tissues. *Cancer Immunol. Res.* **3**, 161–172 (2015).
34. M. Wyatt, K. L. Greathouse, Targeting dietary and microbial tryptophan-indole metabolism as therapeutic approaches to colon cancer. *Nutrients* **13**, 1189 (2021).
35. X. Z. Sun *et al.*, Alteration of fecal tryptophan metabolism correlates with shifted microbiota and may be involved in pathogenesis of colorectal cancer. *World J. Gastroenterol.* **26**, 7173–7190 (2020).
36. L. R. Mourao *et al.*, Protective action of indole-3-acetic acid on induced hepatocarcinoma in mice. *Cell Biochem. Funct.* **27**, 16–22 (2009).
37. Y. Fan *et al.*, The aryl hydrocarbon receptor functions as a tumor suppressor of liver carcinogenesis. *Cancer Res.* **70**, 212–220 (2010).
38. K. Hezaveh *et al.*, Tryptophan-derived microbial metabolites activate the aryl hydrocarbon receptor in tumor-associated macrophages to suppress anti-tumor immunity. *Immunity* **55**, 324–340.e328 (2022).
39. J. Ni *et al.*, Analysis of the relationship between the degree of dysbiosis in gut microbiota and prognosis at different stages of primary hepatocellular carcinoma. *Front. Microbiol.* **10**, 1458 (2019).
40. B. B. Williams *et al.*, Discovery and characterization of gut microbiota decarboxylases that can produce the neurotransmitter tryptamine. *Cell Host Microbe* **16**, 495–503 (2014).
41. D. Chen, J. Wu, D. Jin, B. Wang, H. Cao, Fecal microbiota transplantation in cancer management: Current status and perspectives. *Int. J. Cancer* **145**, 2021–2031 (2019).
42. E. N. Baruch *et al.*, Fecal microbiota transplant promotes response in immunotherapy-refractory melanoma patients. *Science* **371**, 602–609 (2021).
43. Y. H. Chen, W. K. Wu, M. S. Wu, Microbiota-associated therapy for non-alcoholic steatohepatitis-induced liver cancer: A review. *Int. J. Mol. Sci.* **21**, 5999 (2020).
44. M. Luo *et al.*, Preventive effect of Lactobacillus reuteri on melanoma. *Biomed. Pharmacother.* **126**, 109929 (2020).
45. C. Gao *et al.*, Gut microbe-mediated suppression of inflammation-associated colon carcinogenesis by luminal histamine production. *Am. J. Pathol.* **187**, 2323–2336 (2017).